ENHANCING SURFACE CHARACTERISTICS OF AA2024-T3 AIRCRAFT ALLOY THROUGH SYNERGISTIC ANODIZATION AND CERIUM CONVERSION COATING. PART I: PERFORMANCE IN MODEL CORROSIVE MEDIUM

Stefania Portolesi[1], Christian Girginov[2],
Stephan Kozhukharov[3,4], Vanya Lilova[4], Plamen Petkov[4]

[1]*University of Calabria, Via Pietro Bucci*
87036 Arcavacata CS, Italy
[2]*Department of Physical Chemistry*
University of Chemical Technology and Metallurgy
8 Kliment Ohridski Blvd., Sofia 1797, Bulgaria
[3]*LAMAR Laboratory, University of Chemical Technology and Metallurgy*
8 Kliment Ohridski Blvd. 1797 Sofia, Bulgaria
[4]*Department of Physics, University of Chemical Technology and Metallurgy*
8 Kliment Ohridski Blvd., Sofia 1797, Bulgaria
E-mail: s.kozhukharov@uctm.edu

ABSTRACT

The present study is devoted to the monitoring of the performance of AA2024-T3 specimens, after the formation of Anodic Aluminum Oxide (AAO) layer and/or deposition of a Ceruim Conversion Coating (CeCC), obtained at 20°C and 50°C, respectively. Although both methods are well described in the literature, there is no sufficient information regarding the effect of their combination on their behaviour in corrosive media. The performance of the respective specimens was elucidated after 24 h of exposure to 3.5 % NaCl model corrosive medium (MCM) by means of Electrochemical Impedance Spectroscopy (EIS) and acquisition of Potentiodynamic Scanning (PDS) curves. Since the combined AAO/CeCC coating primers revealed superior barrier properties, the respective specimens were subjected to long-term corrosion tests of up to 672 h of exposure to the MCM to evaluate their durability. The results revealed the synergistic effect of the combination of the surface treatment procedures on effective corrosion mitigation.

Keywords: AA2024-T3, anodization, cerium conversion coatings, corrosion protection, barrier ability, durability.

INTRODUCTION

Anodization is a relatively simple method that provide excellent possibility for formation of highly textured anodized aluminum oxide (AAO) films, like the obtained by Gonzales-Rovira et al. [1]. The possibility for incorporation of various metals, such as for example: Cu, Ni [2, 3] and Ag [4, 5] is a major advantage of the AAO layer. Indeed, a number of metals, entire molecules [6], crystals [7] and also nanoparticles could be incorporated into the self-ordered porous oxides, as summarized by Brudzisz et al. [8]. In this sense, the incorporation of boehmite [9], silica [10] and carbon [11 - 13] nanoparticles in such AAO structures were reported in recent years.

On the other hand, the advantages of the Cerium Conversion Coatings (CeCC), as successful environmentally acceptable substitutes of the widely used Chromium Conversion Coatings (CCC) were recently emphasized [14 - 16].

The application of Ce-based compounds to mitigate corrosion and to form coating primers still remains a subject of great interest [17 - 27]. Furthermore, as mentioned by Presuel-Moreno et al. [28], cerium compounds can be used as active corrosion protective components for the elaboration of advanced conversion primers [29, 30], epoxide [31], polymethyl methacrylate [32], carbon fiber reinforced plastic [33], superhydrophobic [34, 35], sol-gel derived [36, 37], coordination polymer [38] and CeO_2 loaded

polytetrafluoroethylene coating systems [39]. Ce-based compounds were also implemented as precursors for Ce-modified AAO [40, 41], and Ni/Cu metallic layers [42].

In this sense, special attention to the great importance of the preliminary treatment of Al-based alloys, prior to the actual CeCC deposition is paid by de Frutos et al. [43] and Ping et al. [44]. Subsequently, the application of the anodization process to form a porous AAO matrix suitable for the deposition of a CeCC layer appeared as a rather interesting research object.

The objective of the present research is to determine in what way anodization and deposition of CeCC on AA2024-T3 alloy alter the surface properties and the performance in a model corrosive medium. In this sense, systematic comparative investigations were performed. To assess the influence of the temperature, the CeCC depositions were performed at 20°C, as well as at 50°C. The performance evaluation of the investigated specimens in a model corrosive medium employed two electrochemical methods: Electrochemical Impedance Spectroscopy (EIS) and potentiodynamic polarization scanning (PDS). To gather comprehensive information, the test procedures were divided into: (i) comparative assessment of the barrier ability of all samples after 24 h of exposure to the model corrosive medium and (ii) determination of the durability exhibited by the combined AAO/CeCC layers after exposure periods of 168, 336, 504, and 672 h.

The results obtained indicate a synergistic effect between anodization and subsequent Cerium Conversion Coating (CeCC) layer deposition, as observed through both electroanalytical methods. The latter process can be conducted under moderate conditions, such as room temperature, achieving an optimal combination of surface treatment procedures.

EXPERIMENTAL

Surface treatment procedures

Six pairs of plates (30 x 30 x 2 mm) cut from AA2024 were submitted to various combinations of surface treatments under the following conditions:

Preliminary treatment

It was performed by immersing the samples in a 50 g dm^{-3} NaOH solution at 50°C for 2 min, followed by subsequent vigorous rinsing with both tap and distilled water. This procedure was succeeded by desmutting in diluted with distilled water HNO$_3$ (dilution ratio was 1:1) for 2 min at room temperature. Finally, the samples were again washed with tap and distilled water for about 1 min. Two of the samples (Set 1) were subjected to this procedure only.

Formation of Anodic Aluminum Oxide (AAO) layers

After undergoing the above-described preliminary treatment, some of the samples have been subjected to galvanostatic anodization for 15 min in a 15 wt. % aqueous solution of H$_2$SO$_4$ with applied current density of 15 mA cm^{-2} at 20°C. After anodizing, two samples were separated from the rest and were labelled as (Set 2). The working zones subjected to anodization are circular with a diameter of 23 mm, corresponding to a surface area of 415 mm^2. During the anodic polarization, the evolution of the forming voltage (U$_f$) with time (t) was recorded.

Cerium Conversion Coating deposition

The deposition was performed spontaneously, for 5 min in aqueous mixture with the following composition: 0.025 M CeCl$_3$.7H$_2$O combined with 0.025 M (NH$_4$)$_2$Ce(NO$_3$)$_5$.4H$_2$O. Just prior to the coating depositions, 5 mL of 30 % H$_2$O$_2$ (for each 250 mL of electrolyte) were added.
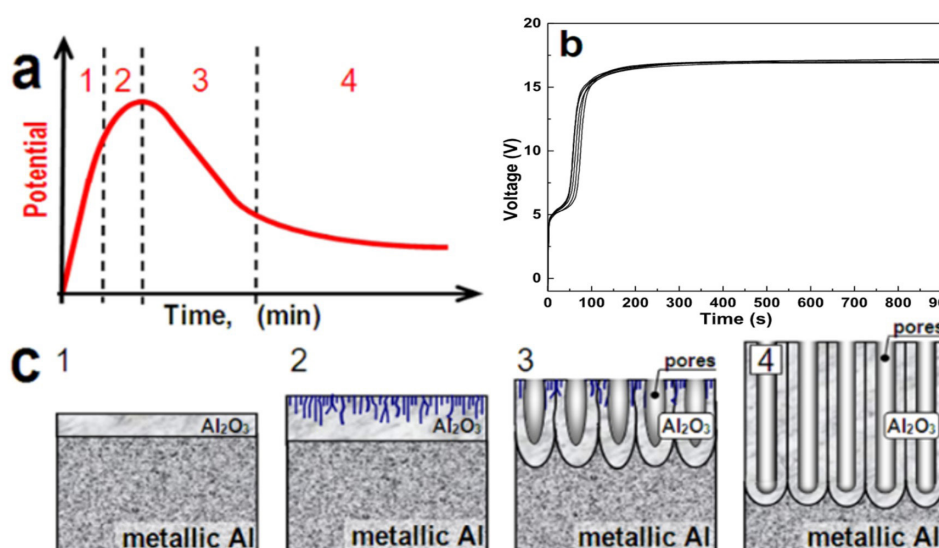
This process was carried out at two temperatures (at 20°C and at 50°C, respectively), on AA2024-T3 samples, with and without preliminary anodization. These CeCC deposition temperatures were selected, since they correspond to the temperatures of the preliminary desmutting, the anodizing (20°C) and the etching (50°C). Besides, the CeCC deposition at 20°C does not require additional energy consumption. For convenience, all samples and respective treatments are summarized in Table 1.

Electrochemical Impedance Spectroscopy (EIS)

The EIS spectra were recorded using a Autolab PGstat 30 (Metrohm), equipped with a Frequency Response Analyzer (FRA-2). The excitation signals were input in the electrochemical cells by a cylindric platinum mesh mounted around the reference electrode, which was Ag/AgCl 3 M KCl type, model 6.0733.100, product of the same producer. The obtained spectra consist of 50 data points distributed in the frequency range from 10 kHz to 0.01 Hz by applying an excitation signal from 10 to

Table 1. Description of the investigated samples and the respective applied procedures abbreviations.

Sample sets	Sample code	Applied procedure			
		Preliminary treatment	Anodization	CeCC deposition	Temperature of CeCC formation
Set 1	$S_{1,1}$, $S_{1,2}$	Yes	Not applied	Not applied	Not applied
Set 2	$S_{2,1}$, $S_{2,2}$	Yes	Yes	Not applied	Not applied
Set 3	$S_{3,1}$, $S_{3,2}$	Yes	Not applied	Yes	20°C
Set 4	$S_{4,1}$, $S_{4,2}$	Yes	Not applied	Yes	50°C
Set 5	$S_{5,1}$, $S_{5,2}$	Yes	Yes	Yes	20°C
Set 6	$S_{6,1}$, $S_{6,2}$	Yes	Yes	Yes	50°C

Fig. 1. Theoretical (a) and actual $U_f(t)$-kinetic curves (b) anodization kinetic curves in galvanostatic mode and illustration of the respective AAO layer formation stages (c).

90 mV, in respect to the open circuit potential (OCP). The respective OCP value was determined immediately before recording each spectrum.

Potentiodynamic Polarization Scanning (PDS)

The PDS curves were acquired in the potential range -50 to +500 mV in accordance with the reference electrode, with a potential sweep of 10 mV s^{-1}.

RESULTS AND DISCUSSION

Procedures for the formation of protective coating primers

For the surface treatment, three procedures (preliminary treatment, anodization and CeCC deposition) were applied under the conditions described in detail in the experimental part. However, only the effects of anodization and CeCC deposition were subjected to detailed analysis, where the samples undergone only pretreatment (Set 1) served as references.

The subsequent anodizing of Set 2 samples involved the simultaneous acquisition of $U_f(t)$-kinetic curves. Examples of typical anodization curves according to the scientific literature review, as well as $U_f(t)$-kinetic curves recorded during the anodization of the Set 2, 5 and 6 samples in the present investigation are shown in Fig. 1.

The theoretical curves, shown in Fig. 1 are described by Girginov et al. [2], based on the literature analysis of several fundamental works [44 - 48]. According to these concepts, the formation of porous AAO layers proceeds in four stages: (1) growth of a dense oxide layer; (2) pore initiation; (3) pore formation and (4) steady-state

oxide growth. However, the actual shapes of the curves acquired during anodization of the preliminary treated samples of the AA2024-T3 alloy in the present case are different. At the very beginning, the potential rises sharply, because the native oxide layer does not possess notable resistance against the 15 % H_2SO_4 electrolyte used. After a retention at about 5 V for almost a minute, the potential increases up to 16.5 - 17.0 V. The curves then become nearly horizontal until the end of the process. Applying Ohm's law and keeping in mind that anodization proceeds under galvanostatic conditions ($j = 15$ mA cm^{-2}) and the above-described voltages, it can be concluded that the resistance of the obtained AAO films reaches values between $R_{AAO}^{min} = 1.100$ and $R_{AAO}^{max} = 1.133$ kΩ cm^2. Hence, the difference between the maximum and the minimum resistance values is $\Delta R = 33$ Ω cm^2. When this value is divided by the average resistance of the AAO layers, it can be concluded that: $\Delta R/R_{av} = (0.033/1.1165) \times 100 = 2.96$ %. Therefore, the difference between the resistance values of the obtained AAO layers is relatively low, indicating the high repeatability of the properties of the obtained AAO layers. Finally, it should be mentioned that the initial retention of the potential for a minute at 5 V is related to consumption of electric current for dissolution of intermetallic inclusions, especially the so-called S-phase inclusions, having Al_2CuMg composition, as was reported in [27, 49, 50].

In the present case (shown in Fig. 1b), the stages of pore initiation (Stage 2) and formation (Stage 3) do not occur. Instead, the curves pass directly from Stage 1 to Stage 4, after the mentioned initial retention of the potential. Consequently, the pore initiation and formation occur between the first and the third minute of anodization. These stages cannot be distinguished by a maximum (unlike the examples in Fig. 1a), because pore formation begins after reaching the thickness of the dense layer. The most probable reasons for the lack of such maximum are the relatively high concentration of the aggressive electrolyte (15 wt. % H_2SO_4) and the considerable current density applied (15 mA cm^{-2}).

Systematic electrochemical characteristics assessment

As described in the experimental part two electrochemical methods, EIS and PDS, were employed for the characterization of the coatings during their exposure to the 3.5 % NaCl model corrosive medium.

The combination of both these methods allowed the evaluation of their corrosion protective properties in the described medium. These properties were divided into barrier ability and durability.

Barrier ability

The comparison of the potentiodynamic scanning (PDS) curves presented in Fig. 2 clearly reveals that the highest barrier ability belongs to the combined AAO/CeCC layers (Sets 5 and 6). Their curves are situated at much lower current densities compared to the rest. In this sense, the curves of the reference samples (Set 1) remain at higher current densities compared to all other types of specimens. This fact indicates the much lower barrier ability of the native oxide layer, compared to the AAO and AAO/CeCC layers, formed during the described procedures.

The PDS curves in Fig. 2 were further subjected to Tafel slope analysis and the obtained results are summarized in Table 2.

The data in Table 2 show some differences between the values of the open circuit potential (OCP) and the corrosion potential (E_{corr}), although theoretically they should be equal. The reason for this difference is that the OCP is measured before the acquisition of the PDS curves, while the E_{corr} values are obtained from its analysis (i.e., after the respective measurement). Therefore, during the PDS measurement, the device polarizes the sample so that the E_{corr} values differ from those of the OCP. The relatively minimal disparities between the OCP and E_{corr} values indicate that the chosen conditions for acquiring the PDS curves do not significantly polarize the electrodes.

According to the pitting nucleation potential (E_{pitt}) and the strength against pitting nucleation (SAPN = E_{corr} - E_{pitt}), defined by Bethencourt et al. [51], no clear trends could be distinguished. However, drastic differences in the polarization resistance (R_p) values are observed. These values for the bare samples (Set 1) are below 10 kΩ cm^2. For comparison, the anodized samples (Set 2) possess R_p values between 115.2 and 156.9 kΩ cm^2. The direct CeCC depositions on the preliminary treated alloy (Sets 3 and 4) practically do not alter the R_p values, as it can be seen from their comparison with those of the references (Set 1).

The highest values of R_p belong to the samples with the combined AAO/CeCC layers (Sets 5 and 6).
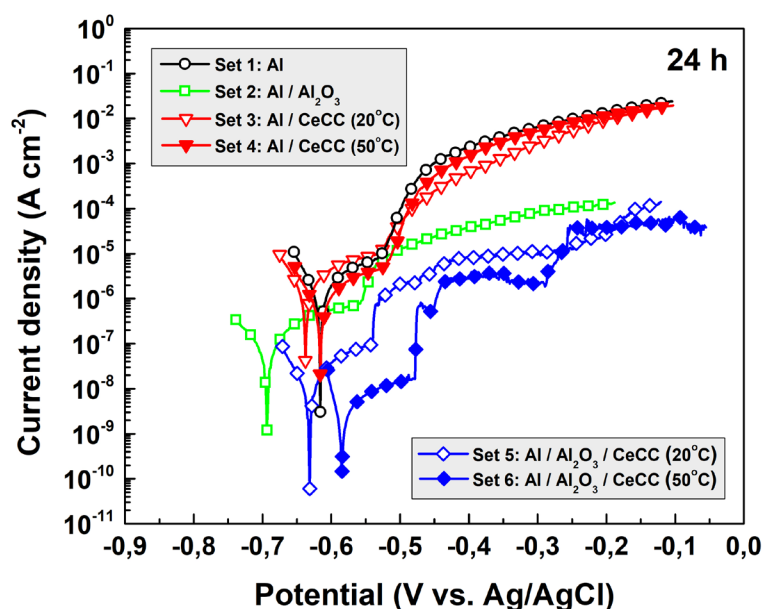
Fig. 2. PDS curves acquired after 24 h of exposure to 3.5 % NaCl model corrosive medium.

Table 2. Values of the electrochemical parameters of the investigated samples.

Sample Set (24h)	Sample	OCP, mV	E_{corr}, mV	E_{pitt}, mV	SAPN, mV	R_p, $k\Omega\ cm^2$
Set 1	$S_{1,1}$	-604	-616	-535	-81	8.35
	$S_{1,2}$	-626	-639	-536	-103	6.44
Set 2	$S_{2,1}$	-689	-694	-559	-135	156.90
	$S_{2,2}$	-662	-668	-541	-127	115.20
Set 3	$S_{3,1}$	-625	-637	-536	-101	6.71
	$S_{3,2}$	-626	-636	-528	-108	6.70
Set 4	$S_{4,1}$	-615	-626	-526	-100	6.85
	$S_{4,2}$	-603	-616	-526	-90	13.83
Set 5	$S_{5,1}$	-701	-631	-540	-91	944.30
	$S_{5,2}$	-687	-694	-526	-168	842.00
Set 6	$S_{6,1}$	-631	-651	-450	-122	5919.00
	$S_{6,2}$	-555	-585	-479	-106	4044.00

Their R_p values are orders of magnitude higher than those of the other sample types, consequently their barrier properties are notably superior. Indeed, the R_p values of the combined layers formed at 20°C, are one order of magnitude higher than those of the AAO layers (Set 2). The formation of CeCC on AAO layer at 50°C results in even higher R_p values, reaching values around 6 MΩ cm² (Set 6).

Clear differences can be seen in the Nyquist plots (Fig. 3a). It is obvious that the combined AAO/CeCC layers have much higher resistance values compared to the other types of samples. This fact indicates the occurrence of a synergistic effect between the anodization and the CeCC formation on the barrier ability of the obtained AAO/CeCC coating primers.

This effect probably results from the interactions between the AAO and CeCC layers. On the one hand, the porous AAO layer serves as a reinforcing matrix

for CeCC. On the other hand, the CeCC layer seals the cavities and pore openings of the AAO layer. Therefore, the combined AAO/CeCC layer possesses a rather enhanced barrier ability due to the contribution of both layer deposition techniques (the formation of AAO by means of anodization and CeCC by spontaneous deposition).

The comparison between the spectra in the Bode plots (Fig. 3b) shows that the values of log|Z| at 10

mHz for the anodized samples with subsequent CeCC deposition reaches 6.5, while those of the anodized only samples (Set 2) lie slightly above 5 and around 4 for the reference samples (Set 1). In other words, the total impedance values differ by orders of magnitude between sample types. At this frequency, its average values (in Ω cm^2) are: 4.266×10^6; 8.475×10^5; 2.027×10^5 and only 1.306×10^4 for sets 6, 5, 2 and 1, respectively. Furthermore, the phase shift vs. frequency plots
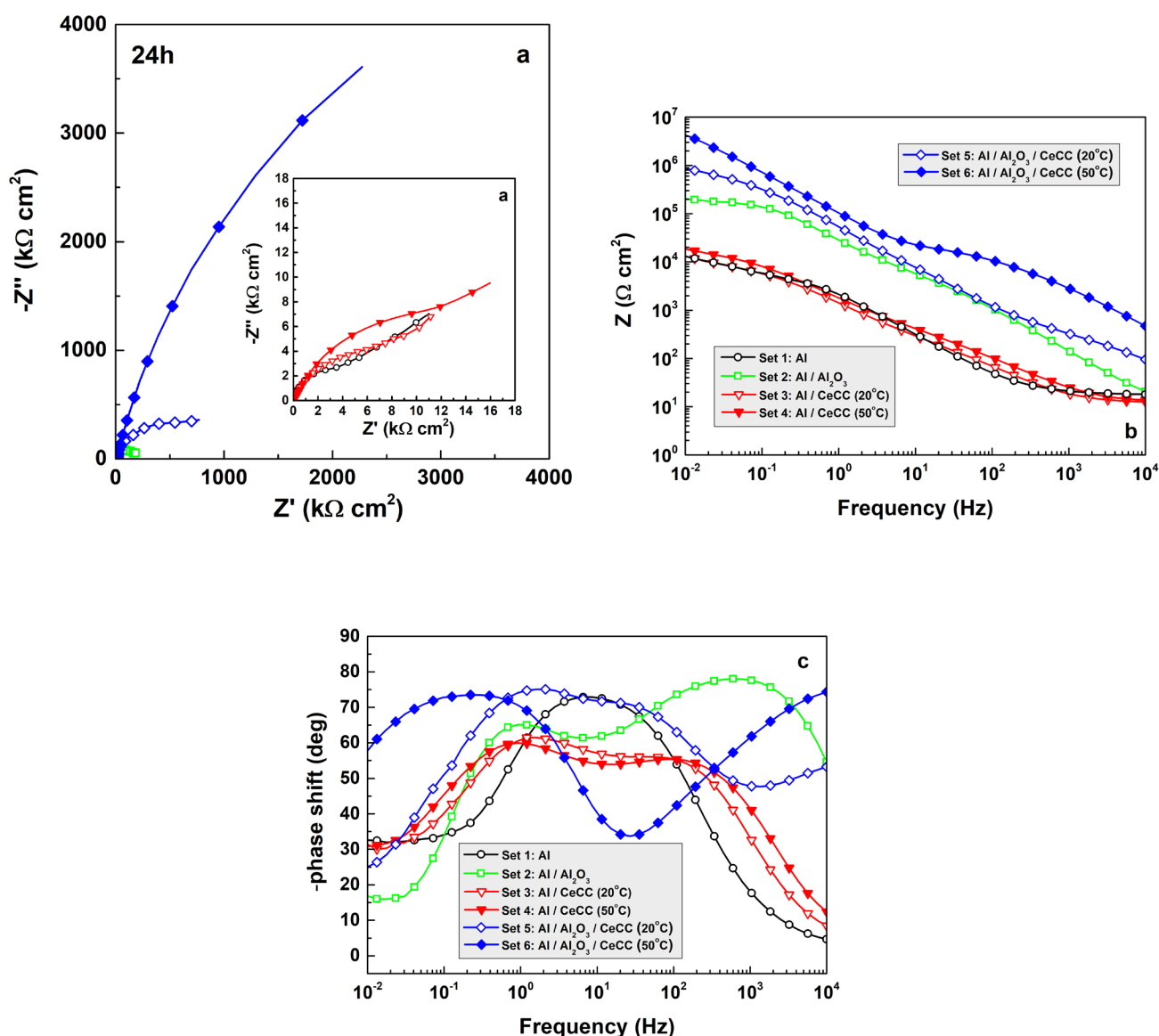

Fig. 3. EIS spectra of the specimens after different surface treatment procedures, acquired after 24 h of exposure to model corrosive medium.
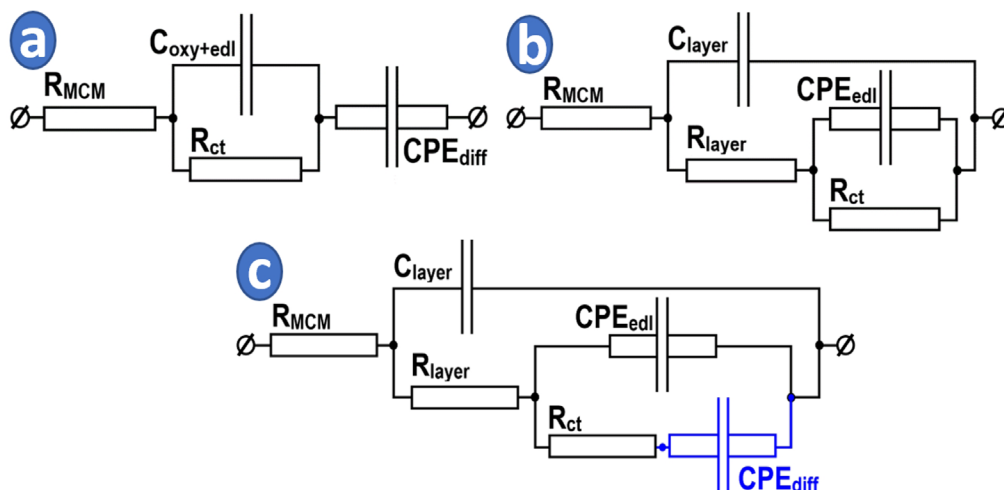
Fig. 4. Model equivalent circuits used for EIS data fitting of the spectra.

(Fig. 3c) reveal the appearance of two clear maxima corresponding to two distinguishable time constants. For comparison, the reference samples have only one maximum, whose appearance is result of the native oxide layer formed on the AA2024-T3 substrates after the preliminary treatment. Their capacitance cannot be distinguished from that of the electric double layer, so their maxima overlap. In turn, the phase shift/frequency dependence of the AAO and AAO/CeCC coatings show the occurrence of additional protective layers, notable by the presence of a second maximum.

The clear differences between the spectra recorded from the samples of the different sets require the use of different model equivalent circuits (MEC) for the interpretation of EIS data. The respective MECs were composed, following the basic rules, postulated in the fundamental work of Zheludkevich et al., and are presented in Fig. 4 [52].

Experience shows that the completely different spectra of the bare alloy samples (Set 1) and these of the other sets require different MECs for their interpretation. All the proposed circuits have R_{MCM} elements related to the resistance of the 3.5 % NaCl model corrosive environment. Electrochemical corrosion processes are represented by the charge transfer resistance (R_{ct}).

However, as already mentioned, in the case of the bare alloy specimens (Set 1), the native oxide layer formed after the preliminary treatment and the electric double layer have indistinguishable capacitances. For

this reason, only one capacitor element for both layers, assigned as $C_{oxy+edl}$, was used (Fig. 4a). Finally, in some cases, a constant phase element for the diffusion processes (CPE_{diff}) on the samples' surface in the MCM was used, commented in the next paragraph.

The additional AAO and CeCC layers on the other types of samples demand three additional elements: CPE_{edl}, C_{layer}, and R_{layer}. The CPE_{edl} element serves for the description of the electric double layer formed between the sample's surface and the model corrosive medium. The C_{layer} component describes the capacitance resulting from the insulating properties of the Al_2O_3, making up the AAO film and the Ce-oxides and hydroxides, composing the CeCC layer. The R_{layer} element describes the resistance of those parts of the MCM that have already penetrated the defects, cracks and pores of the CeCC and AAO layer.

These MECs have been employed for the quantitative analysis of the components of the EIS spectra for all samples, and the fitting results of the EIS data are summarized in Table 3.

The analysis of the data in Table 3 shows that there is no clear difference between the R_{MCM} values for the different sample types. That is because all experiments were performed in the same medium (aqueous 3.5 % NaCl solution). However, a considerable variation in the values of the charge transfer resistance R_{ct} for the respective sets of samples is notable. For the reference samples (Set 1) this value is below 4 kΩ cm^2, whereas the

Table 3. Values of the MEC elements, of the EIS spectra acquired after 24 hours of exposure to MCM.

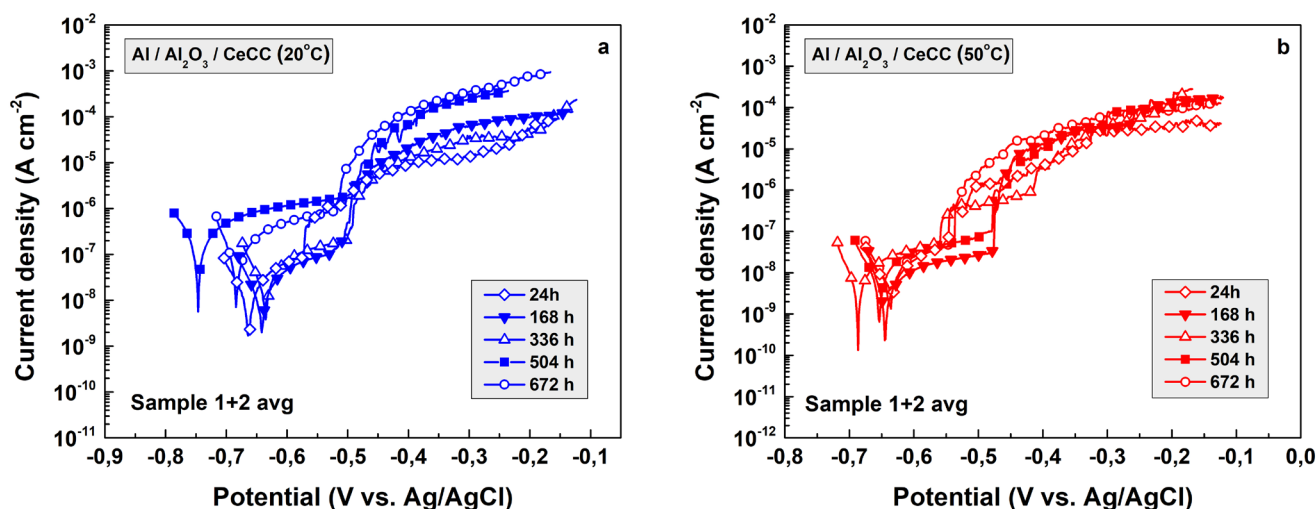| MEC component	Sample	Sample Set					
		Set 1	Set 2	Set 3	Set 4	Set 5	Set 6
R_{MCM}, Ω cm^2	S_1	16.82 ± 0.49	13.17 ± 1.11	13.05 ± 0.25	12.31 ± 0.21	41.50 ± 4.29	32.60 ± 3.75
	S_2	11.44 ± 0.23	12.94 ± 1.14	10.41 ± 0.15	14.33 ± 0.40	16.04 ± 1.49	88.70 ± 10.66
C_{layer}, μF cm^{-2}	S_1	———	1.13 ± 0.03	14.79 ± 0.56	6.12 ± 0.39	$(226.80 \pm 11.09)10^{-3}$	$(263.50 \pm 7.99)10^{-3}$
	S_2	———	1.01 ± 0.03	14.07 ± 0.58	6.34 ± 0.48	$(713.00 \pm 32.47)10^{-3}$	$(132.70 \pm 7.65)10^{-3}$
$C_{oxy+edl}$, μF cm^{-2}	S_1	85.30 ± 3.04	———	———	———	———	———
	S_2	136.30 ± 3.62					
R_{layer}, $k\Omega$ cm^2	S_1	———	0.58 ± 0.30	0.06 ± 0.01	0.05 ± 0.01	0.30 ± 0.01	0.90 ± 0.06
	S_2	———	0.61 ± 0.18	0.03 ± 0.01	1.95 ± 0.93	0.26 ± 0.01	0.66 ± 0.03
CPE_{edl} 10^{-7}, s^n Ω^{-1}cm^{-2}	S_1	———	63.50 ± 2.74	$(16.69 \pm 0.66)10^2$	$(10.90 \pm 0.21)10^2$	38.05 ± 0.68	19.19 ± 0.37
	S_2	———	72.35 ± 3.33	$(14.73 \pm 0.40)10^2$	432.80 ± 66.35	29.43 ± 0.72	23.27 ± 0.46
n	S_1	———	0.76 ± 0.01	0.69 ± 0.01	0.69 ± 0.01	0.82 ± 0.01	0.85 ± 0.01
	S_2	———	0.68 ± 0.01	0.69 ± 0.01	0.63 ± 0.01	0.80 ± 0.01	0.86 ± 0.01
R_{ct}, $k\Omega$ cm^2	S_1	3.79 ± 0.15	214.30 ± 9.18	13.15 ± 1.66	7.28 ± 0.29	922.00 ± 29.24	$(14.71 \pm 3.05)10^3$
	S_2	3.83 ± 0.12	147.70 ± 6.37	9.22 ± 0.60	2.31 ± 1.10	954.00 ± 34.36	$(18.11 \pm 8.98)10^3$
CPE_{diff} 10^{-5}, s^n Ω^{-1}cm^{-2}	S_1	56.09 ± 2.13	———	141.80 ± 92.58	94.09 ± 10.65	———	———
	S_2	92.12 ± 3.77	———	142.70 ± 44.10	11.33 ± 0.39	———	———
n	S_1	0.65 ± 0.01	———	0.74 ± 0.20	0.61 ± 0.04	———	———
	S_2	0.69 ± 0.01	———	0.67 ± 0.03	0.61 ± 0.01	———	———

Fig. 5. Averaged PDS curves acquired after different times of exposure to 3.5% NaCl MCM for samples of: (a) Set 5 and (b) Set 6.

AAO layers (Set 2) possess entire orders of magnitude higher R_{ct} values: between 147 and 214 kΩ cm^2. The direct CeCC formation on the preliminary treated AA2024-T3 alloy at 20°C (Set 3) and at 50°C (Set 4) results in R_{ct} values of the same order as the references (Set 1). The highest R_{ct} values belong to the combined AAO/CeCC coating primers. Depending on the CeCC formation temperature, these values tend towards $R_{ct} \approx$ 1 MΩ cm^2 (Set 5), approaching the range $R_{ct} \approx 15 \div 18$ MΩ cm^2 (Set 6).

Durability

Since the combined AAO/CeCC layers revealed a rather superior barrier ability compared to the other sample types, only representatives of these sample sets are commented below. The averaged PDS curves acquired after different exposure times to the MCM for both types of AAO/CeCC layers, obtained at 20°C (Set 5) and at 50°C (Set 6), are presented in Fig. 5.

All curves in Fig. 5 reveal pitting corrosion, regardless of which sample type they belong to. However, their evolution with exposure time is different. For the CeCC layers deposited at 20°C (Set 5), there is a clear difference before and after 336 hours of exposure. Therefore, both curves obtained after 504 and 672 hours remain in the higher current density range compared to the others.

The curves recorded for the CeCC layers, obtained at 50°C (Set 6), are almost indistinguishable. This fact reveals suppression of the corrosion currents during the exposure of the samples to the MCM. Furthermore, with exception of the curve at 336 hours of exposure, all others shift to more positive E_{corr} values.

Some authors recognize this shift of E_{corr} values as "self-healing effect" [53]. However, the cathodic inhibition by Ce^{3+} and Ce^{4+} free ions is not applicable in the present case, because the CeCC layer should be composed by insoluble Ce(III) and Ce(IV) oxides and hydroxides. A much more probable explanation is based on the ability of AAO to re-passivate, forming a new oxide layer on damaged areas. Furthermore, the defects of the AAO/CeCC film are deep (due to the coating thickness) and narrow enough to be easily blocked by corrosion products. Such corrosion products are, for instance, the Keggin's type aluminum polyhydroxy chlorides, such as: $(Al_{13}O_4(OH)_{24}(H2O)_{12})^{7+}$ or $(AlO_4Al_{12}(OH)_{24}(H_2O)_{12})^{7+}$, as proposed in a previous work [54].

Consequently, during the exposure of the anodized samples with CeCC deposition at 50°C (Set 6) to the MCM, new pittings constantly appear and re-passivate, maintaining constant values of the corrosion currents.

All PDS curves acquired from the durability tests were subjected to further Tafel slope analysis. The results are given in Table 4.

Notable fluctuations in the E_{corr} values are observed for both sample types. This fact indicates that the corrosion process does not proceed gradually, but rather

Table 4. Values acquired by Tafel slope analysis for combined AAO/CeCC samples, obtained at 20 °C and 50 °C after different times of exposure to MCM.

Time	Sample set	OCP, mV	E_{corr}, mV	E_{pitt}, mV	SAPN, mV	R_p, kΩ cm²
24h	Set 5	-694	-663	-533	-130	893.55
	Set 6	-593	-618	-465	-114	$(4.98)10^3$
168 h	Set 5	-631	-648	-498	-150	1990.40
	Set 6	-633	-667	-463	-204	$(5.73)10^3$
336 h	Set 5	-624	-640	-491	-149	971.10
	Set 6	-704	-716	-494	-222	$(4.13)10^3$
504 h	Set 5	-693	-710	-454	-257	971.60
	Set 6	-637	-659	-453	-206	$(4.16)10^3$
672 h	Set 5	-667	-682	-503	-180	704.70
	Set 6	-604	-624	-493	-131	$(4.47)10^3$

a competition occurs between the processes of pitting nucleation and re-passivation.

The strength against pitting nucleation (SAPN) values for both sample sets pass through maxima, due to the already mentioned competition between the pitting nucleation and re-passivation. In the case of the CeCC formation at 20°C (Set 5), the SAPN values gradually increase until the 504th h of exposure. For comparison, the samples from Set 6 show a more remarkable increment of these values, reaching a maximum at the 336th h of exposure. This difference in the SAPN values can be explained assuming cracking of the AAO/CeCC layers of Set 6. The accumulation of corrosion products in the cracks of the samples from Set 6 leads to the earlier reaching of the maximum SAPN value, compared to Set 5. However, the maximum registered SAPN value for Set 5 is higher. The reason for this fact is the much smaller number of defects in this case. Hence, the access of the MCM components to the metallic surface is efficiently suppressed, enabling re-passivation of the damaged AAO areas under the cracks.

Finally, after these maxima, the SAPN values decrease again for both sets. This subsequent reduction in SAPN occurs because pits that are not passivated continue to grow, turning into intergranular corrosion [51, 55].

Clear differences are also observed for the evolution of the R_p values of Set 5 and Set 6. The polarization resistance values of the AAO/CeCC layers, formed at the lower temperature (Set 5) tend to 1 MΩ cm², whereas those, formed at 50°C (Set 6) reveal higher R_p values, tending to about 5 MΩ cm². However, the difference between these values is not so pronounced, and considering that the CeCC deposition at 50°C leads to solution precipitation, the spontaneous deposition at 20°C seems more attractive for industrial applications.

The R_p values reach maxima after 168 h of exposure in both cases, due to the more intensive accumulation of corrosion products in the cracks and defects of the AAO/CeCC layer during the initial period of exposure. This process is most probably combined with CeCC swelling due to film hydration.

The Nyquist plots of the EIS spectra (Fig. 6a, b) show a sharp increase in Z'(- Z'') - arcs at 168 h of exposure, confirming the conclusions made regarding the efficient obstructions of the cracks and defects at the initial exposure periods. Further, the recorded arcs of Set 5 are relatively smaller, compared to those of Set 6. Consequently, the former AAO/CeCC layers have a relatively lower resistance, compared to this of the latter. Probably the CeCC layers of Set 5 are thinner than those of Set 6. Thus, the former do not cover completely the intermerallic inclusions.

The corresponding Bode |Z|(f)-plots (Fig. 6b, c) recorded after different exposure times for the two sets are indistinguishable. Besides, there is no notable difference between the respective plots for Set 5 and Set 6, either. Consequently, the resistance values for the respective sets are of the same order of magnitude, as commented in the previous paragraph.

The phase shift (φ)/frequency (f) plots (Fig. 6d, e) reveal the occurrence of more than one maximum for both sets. Their appearance indicates that there are several interfaces in the corresponding AAO/CeCC
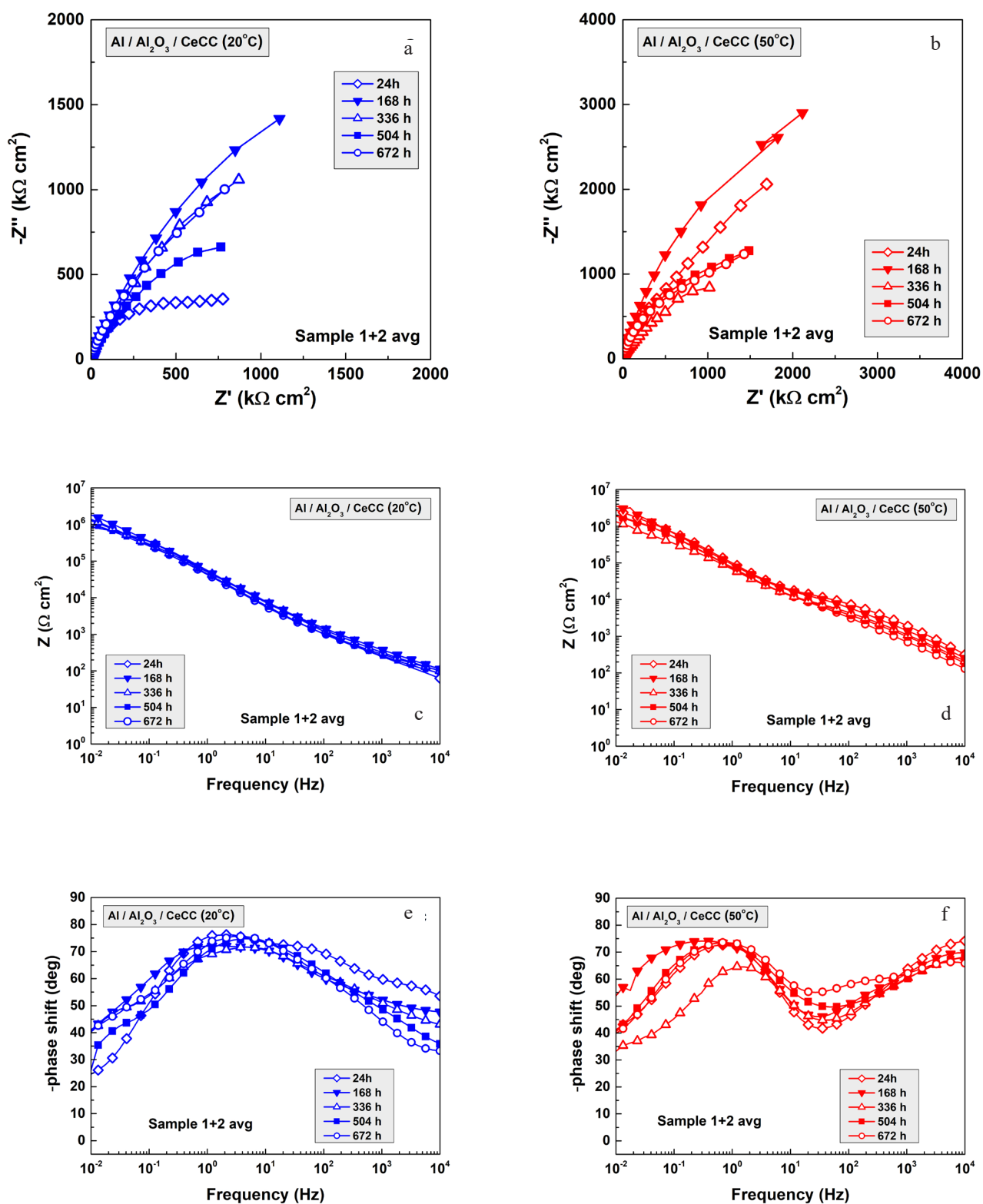
Fig. 6. EIS spectra of combined AAO/CeCC coatings at 20°C (left) or 50°C (right) after different times of exposure to the model corrosive medium.

Table 5. Values acquired by analysis of the recorded EIS spectra of the combined AAO/CeCC layers after different times of exposure to MCM.

Element	Sample	Exposure time				
		24 h	168 h	336 h	504 h	672 h
R_{MCM}, Ω cm^2	Set 5	28.77 ± 4.29	65.35 ± 9.03	60.90 ± 6.95	58.60 ± 5.31	69.75 ± 9.00
	Set 6	60.65 ± 10.66	113.35 ± 24.40	46.55 ± 46.28	57.80 ± 20.60	66.60 ± 14.85
C_{layer}, nF cm^{-2}	Set 5	469.9 ± 32.47	265.15 ± 19.65	265.30 ± 23.48	607.10 ± 59.92	821.95 ± 120.00
	Set 6	198.10 ± 7.99	144.35 ± 6.63	88.35 ± 5.85	83.70 ± 2.87	79.75 ± 3.71
R_{layer}, Ω cm^2	Set 5	284.30 ± 57.00	408.55 ± 41.93	275.90 ± 40.78	287.45 ± 25.44	325.95 ± 42.23
	Set 6	780.67 ± 60.12	1650.01 ± 110.83	790.06 ± 60.09	850.00 ± 110.11	770.09 ± 80.05
CPE_{edl} 10^{-7}, s^n Ω^{-1}cm^{-2}	Set 5	33.74 ± 0.72	40.99 ± 1.61	52.53 ± 2.22	54.66 ± 40.07	70.74 ± 4.33
	Set 6	21.23 ± 0.46	21.81 ± 0.59	11.01 ± 1.28	10.49 ± 0.83	6.01 ± 0.57
n	Set 5	0.81 ± 0.01	0.80 ± 0.01	0.77 ± 0.01	0.82 ± 0.01	0.83 ± 0.01
	Set 6	0.86 ± 0.01	0.86 ± 0.01	0.78 ± 0.01	0.79 ± 0.01	0.77 ± 0.01
R_{ct}, MΩ cm^2	Set 5	0.94 ± 0.36	5.59 ± 0.15	3.25 ± 0.39	1.61 ± 0.18	2.82 ± 0.67
	Set 6	16.41 ± 0.89	19.03 ± 4.60	$(5.20 \pm 0.71)10^{-3}$	$(7.42 \pm 0.83)10^{-3}$	$(6.33 \pm 0.40)10^{-3}$
CPE_{diff} 10^{-7}, s^n Ω^{-1}cm^{-2}	Set 5	-----------------	-----------------	-----------------	-----------------	476.75 ± 123.91
	Set 6	-----------------	-----------------	10.73 ± 1.38	10.98 ± 0.90	9.50 ± 0.62
n	Set 5	-----------------	-----------------	-----------------	-----------------	0.52 ± 0.14
	Set 6	-----------------	-----------------	0.95 ± 0.01	0.94 ± 0.01	0.96 ± 0.01

layers, the capacitances of which are commented below.

The EIS spectra in Fig. 6 were submitted to further analysis by fitting to MECs, shown in Fig. 4b and Fig. 4c. It was established that the circuit in Fig. 4c is more appropriate for the long-term exposure experiments. Thus, the practice has shown that an additional constant phase element is necessary, to describe the notable diffusion processes, which proceed inside the pores and defects of the layers. It was marked as CPE_{diff} and is given in bule in the modified MEC. The obtained results are summarized in Table 5.

Fitting of the EIS data to the MECs has shown that the element CPE_{diff} appears after 168 h of exposure for Set 5, whereas for Set 6, it appears at the end of the entire exposure period. Its appearance coincides with a sharp decay of the R_{ct} values. Consequently, from the data in Table 5 it could be concluded that the AAO/CeCC layers of Set 5 are more durable, despite their lower barrier ability compared to Set 6.

CONCLUSIONS

The present study is a part of systematic research activities, dedicated to the application of rare earth elements for the elaboration of reliable and durable coating primers. The impact of the cerium conversion coating on the surface characteristics of AA2024-T3 alloy samples with and without preliminary anodization was consistently evaluated. For completeness, the CeCC layers were deposited at two different temperatures.

The present research work was completed by performing electrochemical measurements by two independent methods (PDS and EIS) during extended exposure to the model corrosive medium. This approach has enabled to determine both the barrier ability of all investigated samples, and the durability of the specimens that showed best performance.

The PDS curves and EIS spectra acquired after 24 h of exposure to the model corrosive medium have

revealed that the superior barrier ability belongs to the combined AAO/CeCC coating primers. The CeCC deposition on preliminary anodized samples at 50°C additionally enhanced the barrier properties of the resulting combined coating primer. These facts have confirmed the synergism between the applied surface treatment procedures.

In turn, the durability tests have shown that corrosion on the AAO/CeCC covered AA2024-T3 samples proceeds with notable re-passivation of the surfaces. Besides, despite their relatively lower barrier ability the combined AAO/CeCC, formed at 20°C are relatively more durable than those obtained at 50°C.

The most important conclusions from the present research work are related to the occurrence of clear synergism between the anodization and CeCC formation procedures. The layers, formed at 50°C revealed inferior durability compared to those obtained at, 20°C although the higher barrier ability of the former. Hence, the spontaneous CeCC deposition at 20°C could be more attractive from technological point of view, since it does not result in precipitation of the deposition solution.

Acknowledgements

REFERENCES

1. L. González-Rovira, L. González-Souto, P.J. Astola, C. Bravo-Benítez, F.J. Botana, Assessment of the corrosion resistance of self-ordered anodic aluminum oxide (AAO) obtained in tartaric-sulfuric acid (TSA), Surf. Coat. Technol., 399, 2020, 126131. https://doi.org/10.1016/j.surfcoat.2020.126131

2. Ch. Girginov, S. Kozhukharov, A. Tsanev, A. Dishliev, Characterization of Anodized Al 1050 with Electrochemically Deposited Cu, Ni and Cu/Ni and Their Behavior in a Model Corrosive Medium, J. Electrochem. Sci. Technol., 12, 2, 2021, 188-203. https://doi.org/10.33961/jecst.2020.01235

3. Ch. Girginov, S. Kozhukharov, B. Tzaneva, Determination of the Surface Properties of Combined Metal-Oxide Layers, Obtained by AC-Incorporation of Ni and Cu in Preliminary Formed AAO Matrices, Nanoscience and Nanotechnology in Security and Protection against CBRN Threats, 2020, 351-366. https://doi.org/10.1007/978-94-024-2018-0_28

4. S. Kozhukharov, Ch. Girginov A. Tsanev, M. Petrova, Elucidation of the Anodization and Silver Incorporation Impact on the Surface Properties of AA1050 Aluminum Alloy, Journal of the Electrochemical Soc., 166, 10, 2019, C231-C242. https://doi.org/10.1149/2.0461910jes

5. S. Kozhukharov, Ch. Girginov, D. Kiradzhiyska, A. Tsanev, Evaluation of the electrochemical performance of Ag containing AAO layers after extended exposure to a model corrosive medium, J. Electrochem. Sci. Eng., 10, 4, 2020, 317-334. https://doi.org/10.5599/jese.820

6. M. Maksoud, N. Roques, S. Brandès, L. Arurault, J-P. Sutter, Efficient growth of sub-micrometric MOF crystals inside the channels of AAO membranes, J. Mater. Chem. A, 11, 2013, 3688-3693. https://doi.org/10.1039/C3TA01492D

7. M. Gualino, N. Roques, S. Brandès, L. Arurault, J-P. Sutter, From ZIF-8/Al$_2$O$_3$ Composites to Self-Supported ZIF-8 One-Dimensional Superstructures, Cryst. Growth Des., 15, 8, 2015, 3552-3555. https://doi.org/10.1021/acs.cgd.5b00687

8. A.M. Brudzisz, D. Giziński, W.J. Stępniowski, Incorporation of Ions into Nanostructured Anodic Oxides-Mechanism and Functionalities, Molecules, 26, 21, 2021, Art. No. 6378. https://doi.org/10.3390/molecules26216378

9. F. Caubert, P-L. Taberna, L. Arurault, B. Fori, Electrophoretic deposition of boehmite particles to improve the anti-corrosion behavior of anodized aluminum alloy 2024-T3, Bulg. Chem. Commun. 52-E, 2020, 21-27. https://bcc.bas.bg/BCC_Volumes/Volume_52_Special_E_2020/BCC-52-E-2020-21-27-Caubert-04.pdf

10. B. Fori, P-L. Taberna, L. Arurault, J-P. Bonino, C. Gazeau, P. Bares, Electrophoretic impregnation of porous anodic aluminum oxide film by silica nanoparticles, Colloids and Surfaces A,

415, 2012, 187-194. https://doi.org/10.1016/j.colsurfa.2012.09.011

11. P. Ciambelli, L. Arurault, M. Sarno, S. Fontorbes, C. Leone, L. Datas, D. Sannino, P Lenormand, S Le Blond Du Plouy, Controlled growth of CNT in mesoporous AAO through optimized conditions for membrane preparation and CVD operation, Nanotechnology, 22, 2011, 265613. https://doi.org/10.1088/0957-4484/22/26/265613

12. M. Sarno, A. Tamburrano, L. Arurault, S. Fontorbes, R. Pantania, L. Datas, P. Ciambelli, M.S. Sarto, Electrical conductivity of carbon nanotubes grown inside a mesoporous anodic aluminium oxide membrane, Carbon 55, 2013, 10-22. https://doi.org/10.1016/j.carbon.2012.10.063

13. A. Khiat, R.H. Poelma, G.Q. Zhang, F. Heuck, F.D. Tichelaar, M. Sarno, P. Ciambelli, S. Fontorbes, L. Arurault, U. Staufer, Mechanical characterization of individual polycrystalline carbon tubes for use in electrical nano-interconnects, Microelectronic Engineering, 98, 2012, 317-320. https://doi.org/10.1016/j.mee.2012.07.087

14. P. Rajendran, A. Muthuraj, N.E. Rajagounder, Review on CeO_2-Based Corrosion Coatings, Transact Indian Ceram Soc., 81(4), 2022, 158-174. https://doi.org/10.1080/0371750X.2022.2149623

15. C.E. Castano, M.J. O'Keefe, W.G. Fahrenholtz, Cerium-based oxide coatings, Curr Opin Solid State Mater Sci., 19, 2015, 69-76. https://doi.org/10.1016/j.cossms.2014.11.005

16. T. Zehra, M. Kaseem, Lanthanides: The Key to Durable and Sustainable Corrosion Protection, ACS Sustainable Chemistry and Engineering, 11, 18, 2023, 6776-6800. https://doi.org/10.1021/acssuschemeng.3c00763

17. M.A.A. Khan, O.M. Irfan, F. Djavanroodi, M. Asad, Development of Sustainable Inhibitors for Corrosion Control, Sustainability, 14, 2022, Art. No. 9502, 1-17. https://doi.org/10.3390/su14159502

18. R.K. Harcheganiz, A.R. Riahi, Effect of Cerium Chloride on the Self-Corrosion and Discharge Activity of Aluminum Anode in Alkaline Aluminum-air Batteries, J. Electrochem. Soc., 169, 2022, 030542. https://doi.org/10.1149/1945-7111/ac5c06

19. I. Milošev, B. Kapun, P. Rodič, The Relation Between the Microstructure of Aluminum Alloy 7075-T6 and the Type of Cerium Salt in the Formation of the Cerium Conversion Layer, J. Electrochem. Soc., 169, 2022, 091501. https://doi.org/10.1149/1945-7111/ac8d35

20. M.A. El-Hashemy, A.E. Hughes, T. Gengenbach, A.M. Glenn, I.S. Cole, Combined influence of Ce(III) and iodide ions for corrosion protection of AA 2024-T3 in acidic to neutral chloride-rich environments: Electrochemical and surface characterization studies, Journal of Rare Earths, 41, 2, 2023, 309-320. https://doi.org/10.1016/j.jre.2022.05.014

21. P. Rodic, M. Lekka, F. Andreatta, I. Milošev, L. Fedrizzi, The synergistic effect of cerium acetate and sodium sulphate on corrosion inhibition of AA2024-T3 at various temperatures, Electrochim. Acta, 370, 2021, Art. No. 137664. https://doi.org/10.1016/j.electacta.2020.137664

22. M. Kurtela, V. Šimunović, I. Stojanović, V. Alar, Effect of the cerium (III) chloride heptahydrate on the corrosion inhibition of aluminum alloy, Mater. Corros., 71(1), 2020, 125-147. https://doi.org/10.1016/j.porgcoat.2019.105428

23. B. Jegdić, B. Bobić, B. Radojković, J. Kovačina, D. Marunkić, Synergistic effect of $CeCl_3$ and benzotriazole on corrosion resistance of naturally aged and artificially aged AA2024 aluminium alloy, Transactions of Nonferrous Metals Society of China, 30, 6, 2020, 1478-1490. https://doi.org/10.1016/S1003-6326(20)65312-2

24. B. Jegdić, B. Bobić, S. Linić, Corrosion behaviour of AA2024 aluminium alloy in different tempers in NaCl solution and with the $CeCl_3$ corrosion inhibitor, Mater. Corros., 71, 3, 2020, 352–364. https://doi.org/10.1002/maco.201911219

25. M.A. Iqbal, M. Fedel, Protective Cerium-Based Layered Double Hydroxides Thin Films Developed on Anodized AA6082, Adv. Mater. Sci. Eng., 2020, Article ID 5785393, 12 pages, https://doi.org/10.1155/2020/5785393

26. T.T. Nguyen, C. Arrighi, T.T. Thai, L. Dangreau, M.F. Gonon, A.T. Trinh, M.-G. Olivier, Inhibitive effect of the Ce (III) chloride and nitrate on the corrosion resistance of Zn alloyed sacrificial coatings: Effect of alloying compounds of the sacrificial layer, Electrochim. Acta, 452, 2023, Art. No. 142296. https://doi.org/10.1016/j.electacta.2023.142296

27. P. Rodič, I. Milošev, G.S. Frankel, Corrosion of Synthetic Intermetallic Compounds and AA7075-T6

in Dilute Harrison's Solution and Inhibition by Cerium(III) Salts, J. Electrochem. Soc., 170, 3, 2023, Art. No. 031503. http://doi.org/10.1149/1945-7111/acc0a3

28. F. Presuel-Moreno, M.A. Jakab, N. Tailleart, M. Goldman, J.R. Scully, Corrosion-resistant metallic coatings, Materials Today, 11, 2008, 15-23. https://doi.org/10.1016/S1369-7021(08)70203-7

29. W. Zhan, X. Qian, B. Gui, L. Liu, X. Liu, Z. Li, L. Hu, Preparation and corrosion resistance of titanium–zirconium–ceriumbased conversion coating on 6061 aluminum alloy, Mater. Corros., 71, 3, 2020, 419-4291. https://doi.org/10.1002/maco.201911193

30. O.M. Prada Ramirez, F.M. Queiroz, A.M. Tunes, R.A. Antunes, C.L. Rodrigues, A. Lanzutti, S. Pogatscher, M-G. Olivier, H.G. De Melo, Tartaric-sulphuric acid anodized clad AA2024-T3 post-treated in Ce-containing solutions at different temperatures: Corrosion behaviour and Ce ions distribution, Appl. Surf. Sci., 53430, 2020, 147634. https://doi.org/10.1016/j.apsusc.2020.147634

31. X. Chen, J. Tang, H. Wei, H. Zhang, Y. Tang, X. Zhao, Yu Zuo, Effect of Cerium Tartrate on the Corrosion Resistance of Epoxy Coating on Aluminum Alloy and Its Mechanism, Coatings, 12, 6, 2022, Art. No. 785, 1-16. https://doi.org/10.3390/coatings12060785

32. S.V. Harb, M.S. Rodrigues, T.A.C. de Souza, A. Trentin, M.C. Uvida, D.J. Pochapski, S.H. Pulcinelli, C.V. Santilli, P. Hammer, Smart PMMA cerium oxide anticorrosive coatings: Effect of ceria content on structure and electrochemical properties, Prog. Org. Coat., 161, 2021, 106548. https://doi.org/10.1016/j.porgcoat.2021.106548

33. R. Lopez-Sesenes, J.G. Gonzalez-Rodriguez, J.G. Vera-Dimas, R. Guardian-Tapia, L. Cisneros-Villalobos, Organic and inorganic compounds as corrosion inhibitors to reduce galvanic effect for the hybrid structure AA2024-CFPR, J. Electrochem. Sci. Eng., 12, 2, 2022, 343-358. http://dx.doi.org/10.5599/jese.1126

34. A.M. Semiletov, A.A. Kudelina, Yu.I. Kuznetsov, New prospects in the application of superhydrophobic coatings and corrosion inhibitors, Int. J. Corros. Scale Inhib., 11, 3, 2022, 1388-1400. https://dx.doi.org/10.17675/2305-6894-2022-11-3-28

35. S. Abirami, T. Bharathidasan, S. Sathiyanarayanan, C. Arunchandran, Cerium Stearate Electrodeposited Superhydrophobic Coatings for Active Corrosion Protection of Anodized AA2024-T3, Corrosion Journal, 77, 10, 2021, 1080. https://doi.org/10.5006/3799

36. R. del Olmo, U. Tiringer, I. Milosevic, P. Visser, R. Arrabal, E. Matykina, J.M.C. Mol, Hybrid sol-gel coatings applied on anodized AA2024-T3 for active corrosion protection, Surf. Coat. Technol., 419, 2021, 127251. https://doi.org/10.1016/j.surfcoat.2021.127251

37. T.T. Thai, A.T. Trinha, M-G. Olivier, Hybrid sol–gel coatings doped with cerium nanocontainers for active corrosion protection of AA2024, Prog. Org. Coat., 138, 2020, 105428. https://doi.org/10.1016/j.porgcoat.2019.105428

38. M. Zorainy, D.C. Boffito, M. Gobara, A. Baraka, I. Naeem, H. Tantawy, Synthesis of a novel Ce(III)/melamine coordination polymer and its application for corrosion protection of AA2024 in NaCl solution, RSC Adv., 11, 2021, 6330. https://doi.org/10.1039/d0ra08587a

39. M. Chen, Y. Ma, L. Chen, D. Zhang, H. Zhou, J. Chen, Lubrication, wear resistance and corrosion protection on aluminum alloy toward multifunctional coatings with nano-CeO$_2$ inhibition effect, Prog. Org. Coat., 186, 2024, 108066. https://doi.org/10.1016/j.porgcoat.2023.108066

40. R. del Olmo, M. Mohedano, P. Visser, A. Rodriguez, E. Matykina, R. Arrabal, Effect of cerium (IV) on thin sulfuric acid anodizing of 2024-T3 alloy, J. Mater. Res. Technol., 15, 2021, 3240-3254. https://doi.org/10.1016/j.jmrt.2021.09.117

41. L. Selegård, T. Poot, P. Eriksson, J. Palisaitis, P.O.Å. Persson, Z. Hu, K. Uvdal, In-situ growth of cerium nanoparticles for chrome-free, corrosion resistant anodic coatings, Surf. Coat. Technol., 410, 2021, 126958. https://doi.org/10.1016/j.surfcoat.2021.126958

42. P. Zhang, G. Meng, Y. Wang, B. Lei, F. Wang, Significantly enhanced corrosion resistance of Ni–Cu coating modified by minor cerium, Corros. Commun., 2, 2021, 72-81. https://doi.org/10.1016/j.corcom.2021.07.002

43. A. de Frutos, M. A, Arenas, Y. Liu, P. Skeldon, G.E. Thompson, J. de Damborenea, A. Conde, Influence of pre-treatments in cerium conversion treatment of AA2024-T3 and 7075-T6 alloys, Surf. Coat.

Technol., 202, 16, 2008, 3797-3807. https://doi.org/10.1016/j.surfcoat.2008.01.027

44. W. Pinc, S. Geng, M. O'Keefe, W. Fahrenholtz, T. O'Keefe, Effects of acid and alkaline based surface preparations on spray deposited cerium based conversion coatings on Al 2024-T3, Appl. Surf. Sci., 255, 2009, 4061-4065. https://doi.org/10.1016/j.apsusc.2008.10.110

45. G.E.Thompson, Y. Xu, P. Skeldon, K. Shimizu, S.H. Han, G.C. Wood, Anodic oxidation of aluminium, Philosophical Magazine B, 55, 6, 1987, 651-667. https://doi.org/10.1080/13642818708218371

46. G.E. Thompson, Porous anodic alumina: fabrication, characterisation and applications. Thin Solid Films, 297, 1997, 192-201. https://doi.org/10.1016/S0040-6090(96)09440-0

47. H. Takahashi, M. Chiba, Role of anodic oxide films in the corrosion of aluminum and its alloys, Corros. Rev., 36, 1, 2017, 35-54. https://doi.org/10.1515/corrrev-2017-0048

48. G. Amsel, D. Samuel, The mechanism of anodic oxidation, J. Phys. Chem. Sol., 23, 12, 1962, 1707-1718. https://doi.org/10.1016/0022-3697(62)90208-1

49. A.E. Hughes, C. Mac Rae, N. Wilson, A. Torpy, H.T. Muster, A.M. Glenn, Sheet AA2024-T3: a new investigation of microstructure and composition, Surf. Interphase Anal., 42, 2010, 334-338. https://doi.org/10.1002/sia.3163

50. M. Olgiati, P.J. Denissen, S.J. Garcia, When all intermetallics dealloy in AA2024-T3: Quantifying early stage intermetallic corrosion kinetics under immersion, Corros. Sci., 192, 2021, Art. No. 109836. https://doi.org/10.1016/j.corsci.2021.109836

51. M. Bethencourt, F.J. Botana, J.J. Calvino, M. Marcos, M.A. Rodriguez-Chacon, Lanthanide compounds as environmentally-friendly corrosion inhibitors of aluminium alloys: a review, Corros. Sci., 40, 1998, 1803-1819. https://doi.org/10.1016/S0010-938X(98)00077-8

52. M.L. Zheludkevich, R. Serra, M.F. Montemor, K.A. Yasakau, I.M. Miranda Salvado, M.G.S. Ferreira, Nanostructured sol-gel coatings doped with cerium nitrate as pre-treatments for AA2024-T3 Corrosion protection performance, Electrochim. Acta, 51, 2005, 208-217. https://doi.org/10.1016/j.electacta.2005.04.021

53. G. Yoganandan, K.Pradeep Premkumar, J.N. Balaraju, Evaluation of corrosion resistance and self-healing behavior of zirconium-cerium conversion coating developed on AA2024 alloy, Surf. Coat. Technol., 270, 2015, 249-258; https://doi.org/10.1016/j.surfcoat.2015.02.049

54. S. Kozhukharov, V. Kozhukharov, M. Wittmar, M. Schem, M. Aslan, H. Caparrotti, M. Veith, Protective abilities of nanocomposite pretreatments containing Al_2O_3 nano-particles loaded by $CeCl_3$. Prog. Org. Coat., 71, 2011, 198-205. https://doi.org/10.1016/j.porgcoat.2011.02.013

55. G.S. Frankel, Tianshu Li, J.R. Scully, Localized Corrosion: Passive Film Breakdown vs Pit Growth Stability, J. Electrochem. Soc., 164, 4, 2017, C180-C181. https://doi.org/10.1149/2.1381704jes